A method for defect repair of MFI-type zeolite membranes by multivalent ion infiltration

Accepted Manuscript

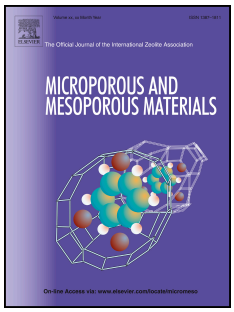

A method for defect repair of MFI-type zeolite membranes by multivalent ion infiltration

Bo Zhu, Xiurong Hu, Jin-Wook Shin, Il-Shik Moon, Yoshito Muraki, Gayle Morris, Stephen Gray, Mikel Duke

PII: S1387-1811(16)30392-4

DOI: 10.1016/j.micromeso.2016.09.011

Reference: MICMAT 7896

To appear in: *Microporous and Mesoporous Materials*

Received Date: 12 May 2016

Revised Date: 7 September 2016

Accepted Date: 8 September 2016

Please cite this article as: B. Zhu, X. Hu, J.-W. Shin, I.-S. Moon, Y. Muraki, G. Morris, S. Gray, M. Duke, A method for defect repair of MFI-type zeolite membranes by multivalent ion infiltration, *Microporous and Mesoporous Materials* (2016), doi: 10.1016/j.micromeso.2016.09.011.

Graphical abstract

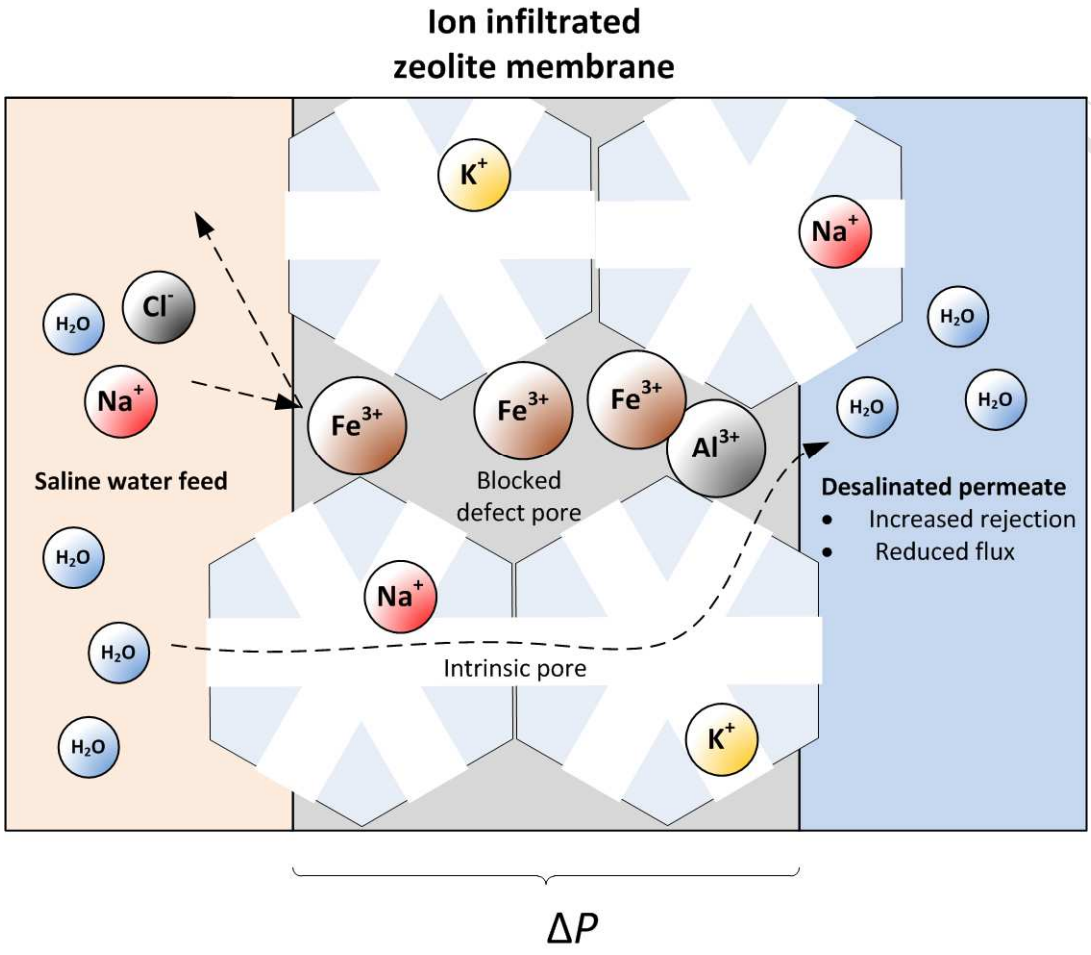

A method for defect repair of MFI-type zeolite membranes by multivalent ion infiltration

Bo Zhu [a], Xiurong Hu [b], Jin-Wook Shin [c], Il-Shik Moon [d], Yoshito Muraki [e], Gayle Morris [f], Stephen Gray [a] and Mikel Duke [a1]

[a] *Institute for Sustainability and Innovation, College of Engineering and Science, Victoria University, Werribee Campus, PO Box 14428, Melbourne, VIC 8001, Australia*

[b] *Chemistry Department, Zhejiang University, Hangzhou, Zhejiang 310028, P. R. China*

[c] *Chosun Refractories Co. Ltd., Taein Dong, Kwangyang-si, Jeonlanam-do 545-893, Republic of Korea*

[d] *Department of Chemical Engineering, Sunchon National University, Maegok Dong, Suncheon 540-742, Republic of Korea*

[e] *C.I. Ceramics (Aust.) Pty. Ltd., Rivulet Crescent, Albion Park Rail 2527, Australia*

[f] *Research Services Office, Flinders University, Adelaide 5001, Australia*

ABSTRACT

MFI-type zeolite membranes are effective for molecular separations, however suffer from non-selective defects. Here we show a means of plugging defects by infiltrating with rigidly bound multivalent ions, and demonstrate improvement to performance as

[1]Corresponding author at: Institute for Sustainability and Innovation, College of Engineering and Science, Victoria University, PO Box 14428, Melbourne, Vic 8001, Australia. Tel: +61 3 9919 7682; fax: +61 3 9919 7696. Email: mikel.duke@vu.edu.au (M. Duke).

salt rejecting (water selective) desalination membranes. Ion uptake into the MFI-type zeolite powder during exposure to a pH 2 solution containing Fe^{3+}, Al^{3+}, Ca^{2+} and Mg^{2+} showed a strong uptake of Fe^{3+} and Al^{3+}. N_2 gas porosimetry showed an increase in micropore proportion, being evidence that adsorbed ions did not enter the intrinsic pores of MFI-type zeolites, instead occupying the larger microporous (grain boundaries) and mesopores. X-ray diffraction (XRD) showed shrinkage in the zeolite crystal, being evidence of loss of monovalent cations within the intrinsic pores supported by the ion uptake results. Zeolite membranes were infiltrated with the solution at 7MPa. Acid and water leaching revealed Fe^{3+} was the most strongly incorporated. This was confirmed by energy-dispersive X-ray spectroscopy (EDS) mapping on the surface of the membrane. The practical effect of the defect repair method was demonstrated on four membranes, where salt rejections in a reverse osmosis experiment were consistently improved (e.g. salt rejection increased from 24% to 84%). Further work should consider benefits to other applications of zeolite membranes including gas separation and pervaporation.

Keywords: *MFI-type zeolite membrane; Ion infiltration; Structure refinement; Defect repair; Desalination performance*

1. Introduction

Desalination is now commonly performed using membrane technology in reverse osmosis (RO) mode. The fundamental requirement of the membrane to carry out desalination by RO is an inherent ability of the membrane to repel ions, but pass water.

While conventional RO membranes made from polyamide are low cost and offer high flux (12–17 $Lm^{-2}h^{-1}$ for seawater with a typical total dissolved solids of 35000 mgL^{-1} at operating pressure of 5.5–6.5 MPa) [1] and excellent ion rejection (up to 99.8% salt rejection) [2], they are not stable under more challenging environments such as heat (>80 °C), oxidants such as chlorine and extremes of pH. Inorganic and organic/inorganic hybrid materials can offer these properties, but the material must possess the essential functional feature to pass water molecules and block ions (i.e. desalination). SAPO-34 (a silicoaluminophosphate with chabazite (CHA) type framework) and ZIF-8 (zeolitic imidazolate framework) have been explored for RO desalination but did not possess the correct structure or integrity to permeate water and reject salts [3]. However inorganic materials which possess these properties are silica [4, 5], hybrid organically bridged silica [6, 7] and zeolites [8-13].

Synthetic zeolite materials have been extensively studied for a variety of applications including catalysis, adsorption, sensing and separation [14-23]. Significant progress in the preparation and characterisation of zeolite membranes has stimulated research in their application for various molecular level separations including gas phase and liquid phase mixtures. Zeolite materials are also promising candidates for filtration of aqueous solutions, where their small pores enable a functional property to diffuse water but reject organics and/or ions [17, 22]. In these applications, their chemical robustness makes them ideal candidates for more durable operation and simplified processes.

Several research groups have explored the possibility of using MFI-type zeolite membranes for their unique open structural properties to achieve salt rejection for

desalination application [2, 12, 17-21, 24-26]. The MFI-type zeolite has orthorhombic crystal symmetry with nearly cylindrical, 10-member ring channels. The aperture size of the MFI-type zeolite is around 0.56 nm [19], which is smaller than the sizes of hydrated ions but larger than the kinetic diameter of water as shown in Table 1 [27]. Recent studies showed that MFI-type zeolites had dynamic behaviour when interacting with different ion complexes (e.g. seawater), and thus caused a change in structure and porosity that could impact on diffusion properties of this material when used as a desalination membrane [28, 29]. For example, monovalent cations (e.g. K^+, Na^+) can uniquely enter the zeolite lattice pores, while divalent cations (e.g. Ca^{2+}, Mg^{2+}) can be absorbed into the grain boundaries of zeolites.

Table 1 Kinetic diameter of water and hydrated ions [27].

Ion	**Hydrated diameter (nm)**
H_2O	0.276
K^+	0.662
Cl^-	0.664
Na^+	0.716
SO_4^{2-}	0.758
Ca^{2+}	0.824
Mg^{2+}	0.856
Fe^{3+}	0.914
Al^{3+}	0.950

Performance testing has demonstrated that MFI-type zeolite membranes working in reverse osmosis (RO) mode are able to deliver high ion rejections; for example, a high rejection (>93%) was achieved for Ca^{2+}, Mg^{2+} and Na^+ from a 0.3wt% seawater solution

at 700 kPa [25], and Na^+ rejection was measured at 99.4% at 2.76 MPa for 0.1 M NaCl solution (5,840 mg L^{-1}, or approximately 9,150 µS cm^{-1}) [12]. Recently, researchers have also attempted to treat synthetic industrial solutions using MFI-type zeolite membranes [11, 12]. These studies showed that MFI-type zeolite membranes had great potential for separation of dissolved organics from aqueous solution, as an example an organic rejection of 99.5% was achieved for 100 ppm toluene with a water flux of 0.03 $Lm^{-2}h^{-1}$ at an operation pressure of 2.76 MPa [12]. Recent work from our laboratories [2] demonstrated the use of MFI-type zeolite membranes for desalination of saline recycled wastewater, highlighting the possibility of avoiding the costly pre-treatment needed for polymeric RO membranes. The zeolite membrane achieved a salt rejection of 80% and an organic rejection of >90%. The zeolite membrane also withstood 168,000 ppm.h of chlorine exposure demonstrating its high chemical tolerance enabling simplified cleaning and biofouling control techniques. Despite these promising outcomes, to reduce capital cost and increase desalination capacity, flux and rejection of zeolite membranes need to be simultaneously improved. Fluxes have been reported in the range of 0.5–1.4 $Lm^{-2}h^{-1}$ at a pressure of 2.76 MPa [30], which is lower than polymer RO membranes. Zeolite membrane thickness is considered as a potential reason for reduced flux. Zeolite membranes (a few µm thick) [2, 17, 18] are much thicker than commercial RO membranes (0.2 µm) [31, 32]. Membrane resistance to water transport is proportional to the dense skin thickness and hydrophilic property. Some studies have shown that the flux of zeolite membranes could be improved by changing the hydrophobicity of the membrane [30] or by filtering through a thin single crystal zeolite nano-membrane [33]. Improved membrane films must also have sufficiently high quality as flow in defects is responsible for the lost rejection. Therefore

techniques to repair defects may be useful in improving membrane flux and separation performance.

Making intact zeolite membranes reliably is another major issue. The prior studies have identified that multivalent cations cannot enter the intrinsic zeolite pores, while monovalent cations such as K^+ and Na^+ can but are hindered by the inability for the counter ion Cl^- to enter yielding a desalination effect [34]. Trace amounts of multivalent cations such as Ca^{2+} in seawater can occupy the grain boundaries but are also blocked in defect free membranes. Meanwhile larger cations such as Fe^{3+} and Al^{3+} will likely have a strong association with the zeolite structure due to their higher valance and ability to co-ordinate and form rigid networks. This supports the concept that these ions by virtue of their exclusive occupation of large defect pores via multiple co-ordination sites could potentially be utilised to inhibit non selective flux in defect pores but maintain water permeation through the intrinsic pores. In order to infiltrate the cations into the defects, their ability to co-ordinate first needs to be minimised by reducing their interaction with the zeolite by reducing the surface charge which is normally strongly negative for the silica rich zeolite. For silicalite (having no added aluminum) the surface isoelectric point was observed at a pH of 5. Above this value, the zeolite surface was negative, and below this value the surface became very slightly positive [35]. However, the Al_2O_3-supported MFI membranes are generally not Al free in their frameworks despite the use of Al-free synthesis solutions during the membrane preparation [18, 36]. Al can be incorporated into the zeolite framework due to the dissolution of the Al_2O_3 surface in the high concentration of NaOH synthesis solution and solid-state diffusion of Al^{3+} during calcinations [37]. Alumina incorporation into the zeolite (ZSM-5) reduced the charge to negative again, even at the lowest pH measured of 3 (tested up to pH of 12),

however, there appeared to be a slight trend to continue towards a neutral surface as the pH was reduced to less than 3 [35]. Therefore, ion infiltration should be performed at low pH (e.g. <3) where charge value is lowest due to weak charges of the material surface around this low pH value, and the strong charge attraction of the ions within the grain boundaries can be established by returning pH to the membrane's operational value typically around pH 7 where very strong negative charges of the zeolite are observed. The aim of this study is to undertake the first known investigation into the use of infiltrated multivalent ions for the defect repair of zeolite membranes, and demonstrate the effectiveness in membrane desalination reverse osmosis application.

The study was carried out by first exploring the uptake of common low cost multivalent ions Fe^{3+}, Al^{3+}, Ca^{2+} and Mg^{2+} into MFI-type zeolite powders. The change to crystal structure as a result of the ion uptake was analysed by X-ray powder diffraction (XRD), and the porous property was analysed by N_2 porosimetry. In order to confirm the function of defect repair by infiltration of the ions, a MFI-type zeolite membrane was fabricated on top of a tubular α-alumina substrate by seed rubbing [2, 24, 38, 39] and secondary hydrothermal growth [2, 24]. The prepared membrane was infiltrated at high pressure using the ion solution. The strength of the ion association into the zeolite was evaluated by acid solution and water leaching. The infiltrated membrane was then evaluated by gas permeation (H_2 and N_2) and then the repair method was tested for improving reverse osmosis salt rejection performance.

2. Experimental and methods

2.1 Materials

The multivalent ion-rich solution containing Fe^{3+}, Al^{3+}, Ca^{2+}, Mg^{2+}, SO_4^{2-} and Cl^- used for ion infiltration experiments for both zeolite powders and membrane in this study was prepared by adding 138 g $Al_2(SO_4)_3 \cdot 18H_2O$ (AJAX Chemicals, Australia), 205 g $MgSO_4 \cdot 7H_2O$ (Merck, Australia), 58 g $Fe_2(SO_4)_3 \cdot 9H_2O$ (AJAX Chemicals, Australia) and 1.7 g $CaCl_2 \cdot 2H_2O$ (Merck, Australia) into 2 L deionised water (DI water). The solution prepared above was filtered using a 0.45 µm membrane filter to remove undissolved solids prior to ion infiltration experiments. The pH of the pre-filtered solution was measured at 2.03. The MFI-type zeolite powder used for ion infiltration has a Zeta potential of 9.16 mV at pH 2 (measured by a Nano-ZS Zetasizer, Malvern Instruments, UK), where at pH 7.5 it has been measured at -38 mV [20]. Exposure of the zeolite to the ion solution at the measured pH (2.03) therefore provided a surface charge that was ideally weak in order to minimalise the charge attractions and repulsions between the ions and zeolite surface, which maximises the ability for infiltration of the ions into the defects of the entire material.

1 M tetra-propyl ammonium hydroxide (TPAOH) solution and tetraethyl orthosilicate (TEOS) (98%) used for membrane preparation were purchased from Aldrich. The MFI-type zeolite seeds (ZSM-5, SiO_2/Al_2O_3 = 360) used for seed-deposition were supplied by ACS Material, USA. The particle size distribution of the MFI-type zeolite seeds was measured to be between 1,000 nm and 3,000 nm (peaking at ~1,800 nm) [24].

The porous α-Al_2O_3 tubular support (95.7% Al_2O_3, apparent porosity 34.9%, external diameter 15 mm, internal diameter 10 mm, length 25 mm, mean pore size ~12.2 µm) used for the current work was supplied by Chosun Refractories Co. Ltd, Korea.

2.2 Ion infiltration into zeolite powders

Ion infiltration into zeolite powders was carried out by mixing 1 g high silica MFI-type zeolite powder with 5 mL ion solution in a 50 mL centrifuge tube, and shaking in a water bath at room temperature (21 °C) for 48 h. Ion behaviour due to the zeolite was also assessed by exposing them only to DI water. After powder infiltration experiments, the mixture was centrifuged (4000 RPM, 10 min) and supernatant decanted from the powder immediately to avoid any further interactions. The supernatant was analysed for cations (including S) by ICP-OES (Shimadzu ICPE-9000). The ion infiltrated zeolite powders were washed with DI water three times to remove any free solution and oven dried at 80 ºC overnight for further characterisation. The adsorbed amount of cations was estimated from ion concentrations measured by ICP-OES and presented as the amount of ion *i* adsorbed per gram zeolite, $C_{z,i}$, (mmol g^{-1}) according to:

$$C_{z,i} = (C_{b,i,0} - C_{b,i,t}) \cdot V/m_z \quad (1)$$

where $C_{b,i,0}$ is the concentration of ion *i* in the bulk supernatant solution initially, $C_{b,i,t}$ is the concentration of ion *i* in the bulk supernatant solution at the end of the experiment (*t*

= 48 h), both in mmol L^{-1}, m_z is the mass of the zeolite added to the solution (g) and V is the volume of the solution added to the zeolite powder.

2.3 Structural characterisation of powder samples

The original and ion infiltrated zeolite powders (washed) were characterised by XRD and N_2 porosimetry. XRD was performed with D/Max-2550pc X-ray powder diffractometer using CuKα radiation (tube operating at 40 kV and 250 mA) with scintillation detector in the range of 3–90º 2θ with a 0.02º step and 1 second per step counting time. Variable slits (DS and SS) were used and RS slit was 0.15 mm. To investigate the structure changes in three dimensions, structural refinement using the Rietveld method [40] was carried out on the XRD data obtained for the original and multivalent ion solution exposed zeolite samples. All the structure refinements were performed using MDI Jade 9.0 software (Materials Data Inc., USA). N_2 adsorption experiments were carried out using a TriStar 3000 porosity analyser (Micromeritics, USA) at liquid N_2 temperature on samples degassed under vacuum for 4 h at 150 °C. In order to reduce instrumental error, the equipment was calibrated with the carbon black standard sample (specific surface area: 30.6 m^2g^{-1} for multi-points and 29.9 m^2g^{-1} for single-point) supplied along with the instrument prior to testing on the zeolite samples. The specific surface area of the carbon black standard was measured at 30.9 m^2g^{-1} for multi-points and 30.2 m^2g^{-1} for single-point. The error range was around 1%.

2.4 Preparation of MFI-type zeolite membrane

The MFI-type zeolite membrane was coated on the above-mentioned porous α-Al_2O_3 tubular support by a seeded secondary growth technique that has been published elsewhere [2, 24]. In this technique, the seed-deposition was performed by directly rubbing MFI-type zeolite seeds (ZSM-5, SiO_2/Al_2O_3 = 360, ACS Material, USA) onto the α-Al_2O_3 support [38, 39]. Following seed-deposition, hydrothermal secondary growth was carried out in a growth solution of 2 mL of 1 M TPAOH, 2 mL of TEOS and 36 mL DI water at 180 °C for 16 h. After growth, the membrane was washed in deionised water to remove loose precipitate and was then calcined at 500 °C for 4 h.

2.5 Membrane ion infiltration procedure

Infiltration of ions was performed using pressurised filtration of the ion solution through the zeolite membrane. The ion solution was fed to the membrane at an applied pressure of 7 MPa and room temperature (21 °C) in a system similar to that used for desalination test in our previous work [24]. The membrane was installed into the stainless steel membrane housing, and the ion solution was fed at a flow rate of 5 $mLmin^{-1}$ by a high pressure piston pump (Series 1, LabAlliance, USA). The ion infiltration experiments were conducted in a cross-flow setup with the feed solution fed under pressure on the outside and permeating to the inside of the membrane. The ionic strength of the feed and permeated water was measured electrical conductivity (EC) with a portable conductivity meter (Sension 156, HACH). EC has been used in this work to represent the overall salt concentrations. Specific cation concentrations were

analysed by inductively coupled plasma-optical emission spectrometry (ICP-OES) (Shimadzu ICPE-9000). Rejection (r_j) of ion j was calculated by:

$$r_j(\%) = \frac{(c_{j,f} - c_{j,p})}{c_{j,f}} \times 100 \quad (2)$$

where $C_{j,f}$ and $C_{j,p}$ are ICP-OES measured concentrations of ion j (j = Fe^{3+}, Al^{3+}, Ca^{2+}, Mg^{2+} or SO_4^{2-}) in the feed and permeate solutions, respectively. Flux J, ($Lm^{-2}h^{-1}$) was calculated according to:

$$J = \frac{v}{At} \quad (3)$$

2.6 Membrane characterisation

Gas permeation was used to evaluate intactness of the zeolite membrane. Permeation of either He or N_2 was carried out by feeding the gas at 100 kPa to the film-side of the membrane using a simple membrane test system as described in a previous study [24]. Gas permeation testing was conducted at 100 ºC in order to remove adsorbed water from the pores to enable gas probing of the zeolite micropores. Permeation was calculated by normalising the data to the membrane area and pressure drop monitored by a TPI 665 digital manometer (Test Products International, Inc. USA) during the permeation test. Elemental analysis on the membrane surface was performed by energy-dispersive X-ray spectroscopy (EDS) on a CamScan MX2500 microscope (CamScan

Optics, Cambridge, UK). EDS data were collected using an EDAX detector and analysed using EDAX Team software.

3. Results and discussion

3.1 Ion infiltration into zeolite powders

3.1.1 Ion behaviour during infiltration

Table 2 shows the concentration of cations present in the supernatant after mixing the ion solution with MFI-type zeolite powder. The concentrations after mixing the zeolite with DI water are presented first in Table 2 for comparison. DI water picked up K^+ and Na^+ from the zeolite, most likely due to the presence of residual K^+ and Na^+ from zeolite powder sample preparation as NaOH and template TPAOH (which contains K^+) were used in the synthesis solution [28]. Upon exposure of the zeolite to the ion solution, the 'Treated solution' results show dynamic behaviour of the trivalent (Al^{3+} and Fe^{3+}) and monovalent (K^+ and Na^+) cations, while divalent cations (Mg^{2+} and Ca^{2+}) showed little change compared to the original 'Untreated solution'. The results showed a large increase in K^+ and Na^+ in the supernatants, while there was a significant reduction in Fe^{3+} and Al^{3+}. The increase in K^+ and Na^+ from the zeolite powder may be due to exchange with Fe^{3+} and Al^{3+}. Release of K^+ and Na^+ and uptake of divalent ions Mg^{2+} and Ca^{2+} by MFI-type zeolites when exposed to seawater have been observed in previous studies [28, 29]. In the present work, it was observed that K^+ and Na^+ exchanged with Fe^{3+} and Al^{3+} but did not exchange with Mg^{2+} and Ca^{2+}. This suggests

that K^+ and Na^+ in MFI-type zeolites exchange in preference with trivalent ions when both trivalent and divalent cations are present in the solution. From Table 2, the percentage of relative adsorbed cations was estimated to be 42%, 57%, 0% and 0.2% for Al^{3+}, Fe^{3+}, Mg^{2+} and Ca^{2+}, respectively.

Table 2 Ion concentrations of the untreated and zeolite powder treated DI water and multivalent ion solution samples.

Sample	**Al^{3+} (mg L^{-1})**	**Fe^{3+} (mg L^{-1})**	**Mg^{2+} (mg L^{-1})**	**Ca^{2+} (mg L^{-1})**	**Na^+ (mg L^{-1})**	**K^+ (mg L^{-1})**
Untreated DI water	<0.01	<0.05	<0.01	<0.01	<0.01	<0.01
Treated DI water	<0.01	<0.05	<0.01	<0.01	610	190
Untreated solution	6000	4750	9500	150	7	0
Treated solution	5000	3400	9500	145	1350	900

Figure 1 shows the adsorption of major cations from the ion solution when exposed to the MFI-type zeolite powder in terms of their molar quantity normalised to the weight of the zeolite according to Equation 1. The amount of K^+ (0.11 $mmolg^{-1}$) and Na^+ (0.29 $mmolg^{-1}$) released was close to that previous reported for MFI-type zeolite with high Si/Al ratios (up to 0.08 $mmolg^{-1}$ for K^+ and 0.26 $mmolg^{-1}$ for Na^+) after exposure to seawater [29]. The results showed that the total released monovalent ions (K^+ and Na^+) was slightly higher than the total adsorbed amount of multivalents (e.g. Al^{3+} and Fe^{3+}) (molar ratio of monovalents and multivalents ~1.3), suggesting a physical adsorption effect since the molar ratio of monovalent ions (K^+ and Na^+) and trivalent ions (Al^{3+} and Fe^{3+}) should be around 3 if this is a charge functional ion exchange. The preferential uptake of the trivalent cations supports the concept that they were infiltrating the zeolite

and forming strong surface complexes within the material. The next step in this investigation was to confirm the location of the infiltrated ions.

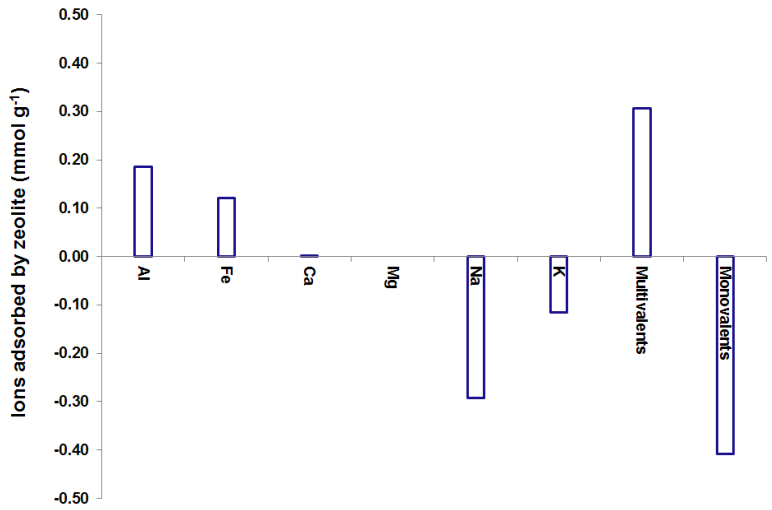

Fig. 1 Moles of the major cations in multivalent ion solution adsorbed after 48 h exposure to zeolites.

It is well known that MFI-type zeolites have an intrinsic pore size of 0.54–0.56 nm [19, 41-43]; but smaller intrinsic pores (e.g. ~0.3 nm), micropores of 1.1–1.2 nm and mesopores > 2.5 nm have also been measured by positron annihilation lifetime spectroscopy (PALS) [28, 29]. Micropores of size between 1 nm and 2.5 nm have been previously detected in silicalite-1 by n-hexane porosimetry [44]. As mentioned earlier, the kinetic diameter of water (0.276 nm, Table 1) is smaller than the intrinsic pore size (e.g. 0.54–0.56 nm) of MFI-type zeolites, so water molecules should be able to physically enter and exit the intrinsic pores. The size of hydrated ions (e.g. K^+ 0.662 nm, Na^+ 0.716 nm, Fe^{3+} 0.914 nm, Al^{3+} 0.950 nm) as shown in Table 1 are larger than the intrinsic pore size (e.g. 0.54–0.56 nm) but smaller than measured micropore (e.g. 1–2.5 nm) and mesopore (>2.5 nm) sizes, suggesting that most of the ion

adsorption and exchange observed due to exposure to multivalent ion solution (Table 2 and Fig. 1) is likely occurring in the 1–2.5 nm micropores and >2.5 nm mesopores. Despite this, molecular dynamics simulation has shown that hydrated Na^+ can enter the intrinsic pores of MFI-type zeolite, but is hindered by the restricted diffusion of the counter ion Cl^- which is repelled by the negatively charged zeolite surface [34]. This is supported by experimental data which shows Na^+ and K^+ diffusion through an MFI-type zeolite membrane upon increase in temperature, explained by the potential widening of the intrinsic pores and/or reduction in size of the hydrated ions enabling diffusion of Na^+, K^+ and Cl^- [25]. Regardless, Fe^{3+} and Al^{3+} are too large to enter the intrinsic pores, so their significant uptake into the zeolite must have occurred within the larger defect pores.

3.1.2 XRD and structure refinement

The XRD patterns (Fig. 2) taken at wavelength of 1.54 Å (CuKα radiation) for the zeolite samples showed a typical MFI-type framework with 2θ around 7.9º, 8.8º, 14.7º, 23.0º, 23.9º and 29.8º for the major peaks '101', '200', '301', '501', '303' and '503', respectively [20, 29, 43]. It was found that the powder samples treated by DI water and multivalent ion solution had the same MFI pattern fingerprint to the original MFI-type zeolite (Fig. 2a), but a slight shift in the most intense Bragg peak (101) was observed in the zeolite samples exposed to DI water and ion solution (Fig. 2b inset). This implies a change in crystal dimension.

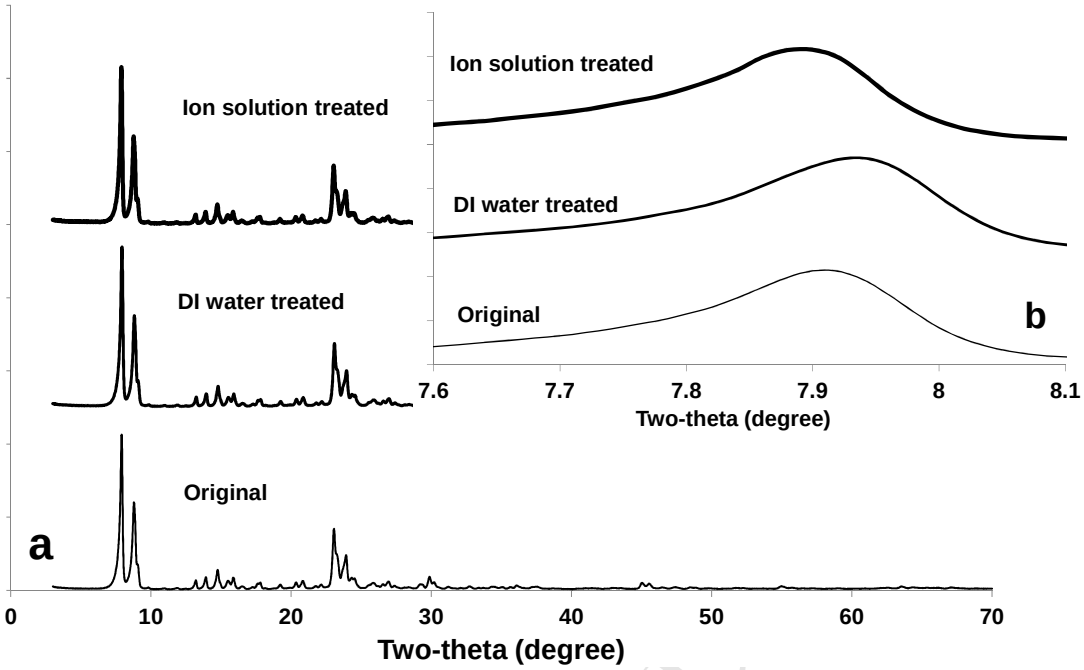

Fig. 2 XRD patterns taken at wavelength of 1.54 Å (CuKα radiation) (a) and differences in the most intense Bragg peak (101) between the zeolite samples.

The fitting patterns of the original MFI-type zeolite powder sample from Rietveld structural refinement are shown in Supplemental Material Figure S1, which confirmed effectiveness of the Rietveld refinement. The unit-cell parameters and volume from Rietveld structural refinement for the MFI-type zeolite powder samples are given in Table 3 and the changes in unit-cell parameters are shown in Figure 3. The unit-cell parameters (a = 2.0044 nm, b = 1.9826 nm, and c = 1.3358 nm) obtained in this study for the original zeolite powder are close to those determined by Van Koningsveld et al (a = 2.0022 nm, b = 1.9899 nm, and c = 1.3383 nm) [45] and Olsen et al (a = 2.007 nm, b = 1.992 nm, and c = 1.342 nm) [46] using the same space group *Pnma*. The structure determined by Van Koningsveld and co-workers [45] is believed to be more accurate and has been used for a thermodynamic study of water intrusion in silicalite by Monte Carlo simulations [47].

The unit-cell parameters and volume of the MFI-type zeolite sample increased after 48 h exposure to DI water compared to the original sample. Unit-cell dimension in a-, b- and c-directions changed 0.79%, 0.78% and 0.76% respectively (Fig. 3) for the zeolite sample exposed to DI water, indicating that expansion occurred in the lattice structure of MFI-type zeolite. Lattice expansion has also been observed in MFI-type zeolites due to exposure to pure water [48] or KCl solution (e.g. 0.05 M) [28]. While the unit-cell dimensions became smaller (Table 3), with a change of -0.75%, -0.71% and -0.67% in a-, b- and c-directions respectively (Fig. 3), after 48 h exposure of the MFI-type zeolite sample to ion solution compared to the original sample. This result indicates that shrinkage occurred in the lattice structure after infiltration of the trivalent ions (and departure of the monovalent ions). Typically, crystals expand in the presence of ions [49], which makes the observation of contraction for the multivalent ion solution exposed zeolites an unusual finding. However, crystal contraction has been observed for zeolites when undergoing dehydration and it was concluded that the presence of ions is responsible for significant deformation of the native zeolite framework upon dehydration [50]. Our material has undergone the opposite treatment. During synthesis, zeolites with Na^+ from NaOH used in synthesis and K^+ from synthesis impurities (found in TPAOH) contracted during calcination to remove the template. Upon 'conditioning' in DI water, the crystal relaxed and expanded upon rehydration with water despite the departure of Na^+ and K^+ as observed in Table 3. Meanwhile with the exposure of the same zeolite material to the ion mixture, the crystals conformed to equilibrium and contracted relative to their deformed state from synthesis to achieve this more relaxed structure. This was also observed when the MFI-type zeolite was exposed to seawater

[29]. While it is not possible to confirm with the present data, uniquely in this case the infiltration of trivalent ions into the defects and enhanced removal of monovalent ions compared to DI water exposure (likely from the intrinsic zeolite pores) led to this more contracted crystal.

Table 3 Unit-cell parameters (nm) and volume (nm^3) of the MFI-type zeolite powders before and after exposure to DI water and multivalent ion solution

MFI-type zeolite	*a*	*b*	*c*	*V*
Original	2.0044(8)	1.9826(8)	1.3358(5)	5.3083
DI Water treated	2.0203(8)	1.9981(8)	1.3459(6)	5.4330
Multivalent ion solution treated	1.9894(8)	1.9685(7)	1.3268(5)	5.1959

*Values in parentheses represent estimated standard deviations in the last quoted place.

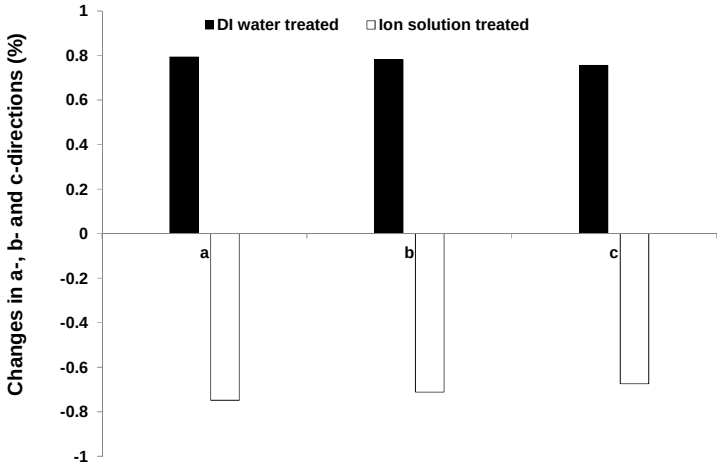

Fig. 3 Unit-cell dimension changes in a-, b- and c-directions after exposure to DI water or multivalent ion solution.

3.1.3 N_2 porosimetry

The adsorption isotherms of N_2 at 77 K for the MFI-type zeolite powders shown in Figure 4 can be classified as type-IV [51] with jump in adsorption at a relative pressure P/P_0 of around 0.2 due to adsorption hysteresis observed in the desorption branch (not shown). The hysteresis loop is due to capillary condensation within mesopores [52]. The uptake of nitrogen at low relative pressures ($P/P_0 < 0.2$) is due to micropore filling [41, 53]. The samples are, therefore, microporous in nature with a contribution from mesopores consistent with the hierarchical structure of zeolites discussed earlier related to intrinsic and defect pores.

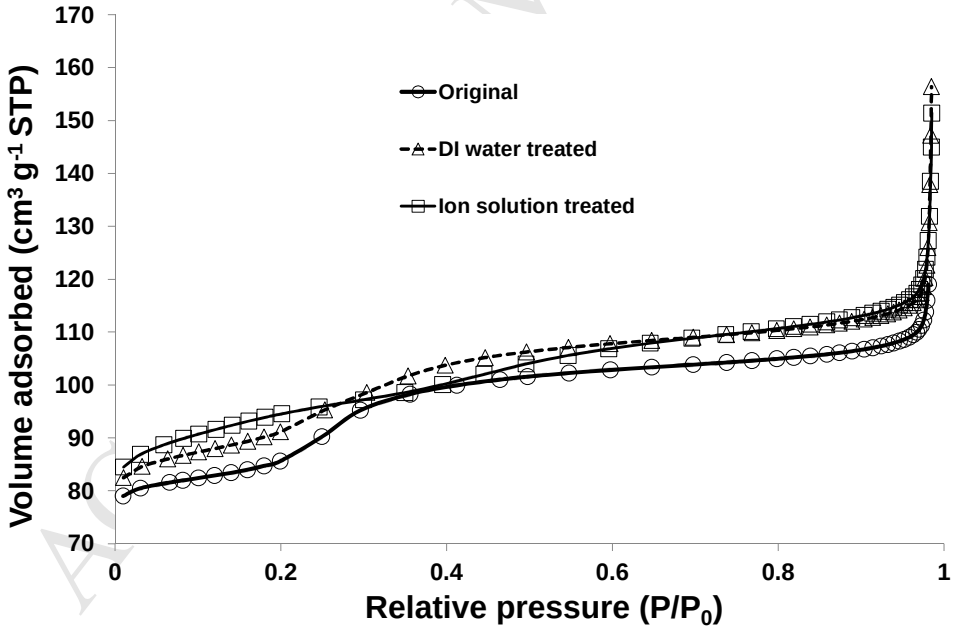

Fig. 4 Adsorption isotherms of N_2 for the original and DI water or multivalent ion solution treated MFI-type zeolite powders at 77 K.

Table 4 compares the changes in BET surface area, t-Plot micropore area and micropore fraction (as measured by N_2 adsorption t-plot analysis relative to BET total area) of the MFI-type zeolite powder samples before and after exposure to DI water or multivalent ion solution. The BET surface area measured for the original MFI-type zeolite (284 m^2g^{-1}) is slightly smaller than that previous reported (~300–330 m^2g^{-1}) [54, 55]. However, the difference between this measured and the reported is in a reasonable range. This difference is likely to be due to the different synthesis conditions performed within different laboratories. It can be seen that only a slight increase in BET surface area was observed for the DI water and ion solution treated MFI-type zeolite powder samples when compared to that of the original MFI-type zeolite. However, there was a significant increase in proportion of micropores after exposure of the MFI-type zeolite powder to DI water or ion solution. This may be due to effects observed above, where both DI water and ion solution exposure led to the departure of monovalent cations from the zeolite that opened up the smaller pore spaces giving the observed increase in micropore proportion. The DI water isotherm appeared to shift uniformly upwards indicating opening of the smallest micropores measured by the first adsorption data point, which added uniformly to all other points on the isotherm. While this increase also occurred for the ion solution exposed zeolite, there was a proportional decline at P/P_0 around 0.4 indicating closure of larger pores, which could be explained by the release of monovalent ions which was in turn accompanied by adsorption of larger multivalent ions that effectively 'closed' the larger micropores. It is possible that large Al^{3+} and Fe^{3+} ions might physically occupy the mesoporous space, thus reducing the mesopore proportion while the departed monovalent ions led to increasing the relative micropore proportion.

Table 4 N_2 adsorption measured BET surface area, t-Plot micropore area and proportion of micropores (t-Plot micropore area×100/ BET surface area) of the MFI-type zeolite powders before and after exposure to DI water or multivalent ion solution.

MFI-type zeolite sample	**BET surface area** (m^2g^{-1})	**t-Plot micropore area** (m^2g^{-1})	**Proportion of micropores** (%)
Original	284	149	52
DI Water treated	293	186	64
Multivalent ion solution treated	293	210	72

3.2 Infiltration of ions into zeolite membrane

Prior to the ion infiltration test, the membrane was first confirmed as having a zeolite coating by measuring rejection of NaCl solution (3,000 mgL^{-1} TDS). The membrane showed an average salt rejection of 31% with a flux of 2 $Lm^{-2}h^{-1}$ measured at 7 MPa pressure drop. This is lower than that expected for zeolite desalination membranes, where >90% salt rejections are expected [12, 25], but shows an intact zeolite coating with some non-selective water flux through defects. This membrane is suitable for investigating ion infiltration.

After testing with NaCl solution, the membrane was flushed with DI water and then fed with the ion solution at 7 MPa and 21°C for 8 hours of similar composition to the 'Untreated solution' in Table 2. EC rejection was 71% and water flux ranged from 0.22 to 0.29 $Lm^{-2}h^{-1}$. Cation analysis of the permeated solution by ICP-OES determined

rejections for the major ions at 99% for Fe^{3+}, 83% for Al^{3+}, 87% for Mg^{2+}, 48% for Ca^{2+} and 80% for SO_4^{2-}. These rejections are higher than NaCl as expected as they are all larger ions in hydrated form as shown in Table 1. It is noted that every ion was detectable in the permeate, including Fe^{3+}, highlighting that all ions had infiltrated through the zeolite film.

3.2.1 Gas permeation testing of ion infiltrated zeolite membrane

Table 5 shows the permeation of single gas (He or N_2) measured for the bare α-Al_2O_3 support, the prepared membrane and the ion infiltrated zeolite membrane. The permeance of He or N_2 for the prepared membrane was two orders of magnitude lower than that of the bare tube, indicating a rate limiting zeolite layer was formed on the surface of the support. The N_2 permeance (3.3×10^{-7} mol m^{-2} s^{-1} Pa^{-1}) measured for the MFI-type zeolite membrane prepared in this work displayed a similar value to those previously prepared in our laboratory by the same seeded secondary growth method (~3.7×10^{-7} mol m^{-2} s^{-1} Pa^{-1}) [2] and that reported in the literature (~3.0×10^{-7} mol m^{-2} s^{-1} Pa^{-1}) [56], but was larger than that prepared by the in-situ method (~0.2×10^{-7} mol m^{-2} s^{-1} Pa^{-1}) [25]. Interestingly the ion infiltrated membrane N_2 permeance was closer to this value, being an order of magnitude smaller than the as synthesised membrane. Clearly infiltration of ions has blocked gas permeation channels in the membrane. While this is a positive sign towards defect blocking, it did not lead to increased He/N_2 permselectivity (permeance ratio between He and N_2) where the value remained unchanged compared to the original membrane, and was smaller than reported by others (~3.0) [56]. Size exclusion selectivity between He (kinetic diameter 0.26 nm) and

N_2 (kinetic diameter 0.36 nm) is not expected in the intrinsic pores (0.56 nm) of zeolite since both gases are smaller than the zeolite pore channels, but Knudsen ideal selectivity of at least 2.6 could be expected. While our application of single gas permeation gave us the ability to rapidly assess the membrane film intactness, we are aware that the permeation test of single gases (He or N_2) can only provide information on the change in gas flow resistance through the membrane, and does not assist in understanding changes to the selective structure. Direct measurement of the pore morphology of the membrane film using techniques such as evaporporometry and nano-permporometry would give a better understanding of the pore size. If there is any benefit of infiltrating the zeolite with the ions to gas or vapour separation, a dedicated study on these applications would be required. However, this work will consider the practical benefits to rejection of salts in saline solutions. For water separation the hydrated ions are larger than the intrinsic zeolite pore channels, so their rejection can be affected by blocking of larger mesoporous defects.

Table 5 Permeation of He and N_2 for the bare α-Al_2O_3 support and prepared zeolite membrane after drying at 100 °C in air for 1 h, and ion infiltrated membrane dried overnight at 100 °C.

Sample	**He permeation (10^{-7} mol m^{-2} s^{-1} Pa^{-1})**	**N_2 permeation (10^{-7}mol m^{-2} s^{-1} Pa^{-1})**	**He/N_2 permselectivity**
Bare tube	1120	745	1.5
Membrane	4.1	3.3	1.2
Ion infiltrated membrane	0.19	0.16	1.2

3.2.2 Binding strength of ions infiltrated in zeolite membrane

The strength of the association of the ions infiltrated into the zeolite membrane was measured by attempting to remove them with acid solution and water. To do this, the membrane was flushed with DI water and then fed with 1 M HCl solution at an applied pressure of 7 MPa and 21 ºC followed by DI water flushing under the same conditions. Figure 5 shows the initial DI water flux and the water flux measured for each DI water permeate (total 3 times, 30 min for each permeation) after 1 M HCl cleaning. The average DI water flux at an applied pressure of 7 MPa and 21 ºC after the HCl (1 M solution) clean was 1.2 L m^{-2} h^{-1}, which was much smaller than that from the initial DI water testing of 5.6 L m^{-2} h^{-1}. This indicates that the water flux was not fully recovered after permeating the acid solution consistent with tight binding of cations in the zeolite membrane.

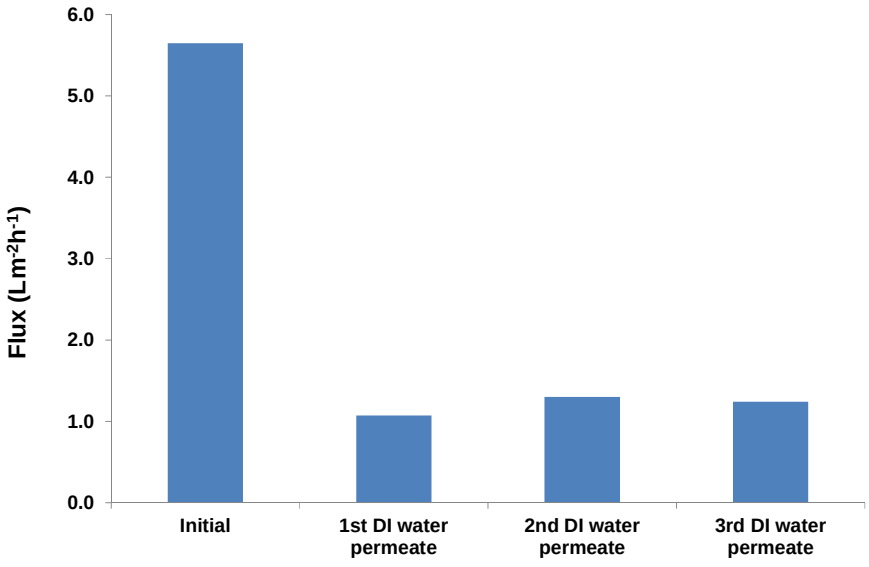

Fig. 5 Comparison of DI water flux measured from each DI water permeate after 1 M HCl cleaning and the initial DI water flux value, applied pressure = 7 MPa.

To further analyse the composition of the ions that may have been removed from the acid treatment, the permeated liquids from 1 M HCl cleaning (HCl permeate) and DI water flushing (1st, 2nd and 3rd DI water permeate) under 7 MPa and 21 ºC were analysed by ICP-OES. Figure 6 shows the ion concentrations measured for Fe^{3+}, Al^{3+}, $Ca^{2+}$and Mg^{2+} in each permeate sample over time. Table 6 compares the absolute amount of the cations (Fe^{3+}, Al^{3+}, $Ca^{2+}$and Mg^{2+}) removed from the multivalent ion solution tested membrane by HCl (1 M solution) cleaning and DI water flushing with those adsorbed by zeolite material in ion infiltration experiments. In order to highlight the relative proportions removed with HCl cleaning and repeated DI water permeation, the concentrations of Fe^{3+}, Al^{3+}, Ca^{2+} and Mg^{2+} were also expressed as weight percentage of the total amount of only these ions in one permeate (Fig. 6 inset). The proportions of the cations in the pre-filtered multivalent ion-rich feed solution were also included in Figure 6 (inset) for comparison. The results (Fig. 6 inset) showed a relatively larger proportion of Al^{3+} present in the permeate samples from all the cleaning steps. Fe^{3+} and Mg^{2+} were consistently lower in proportion to what was originally fed. Ca^{2+} measured for the permeate samples was proportionately high compared to the original multivalent ion solution.

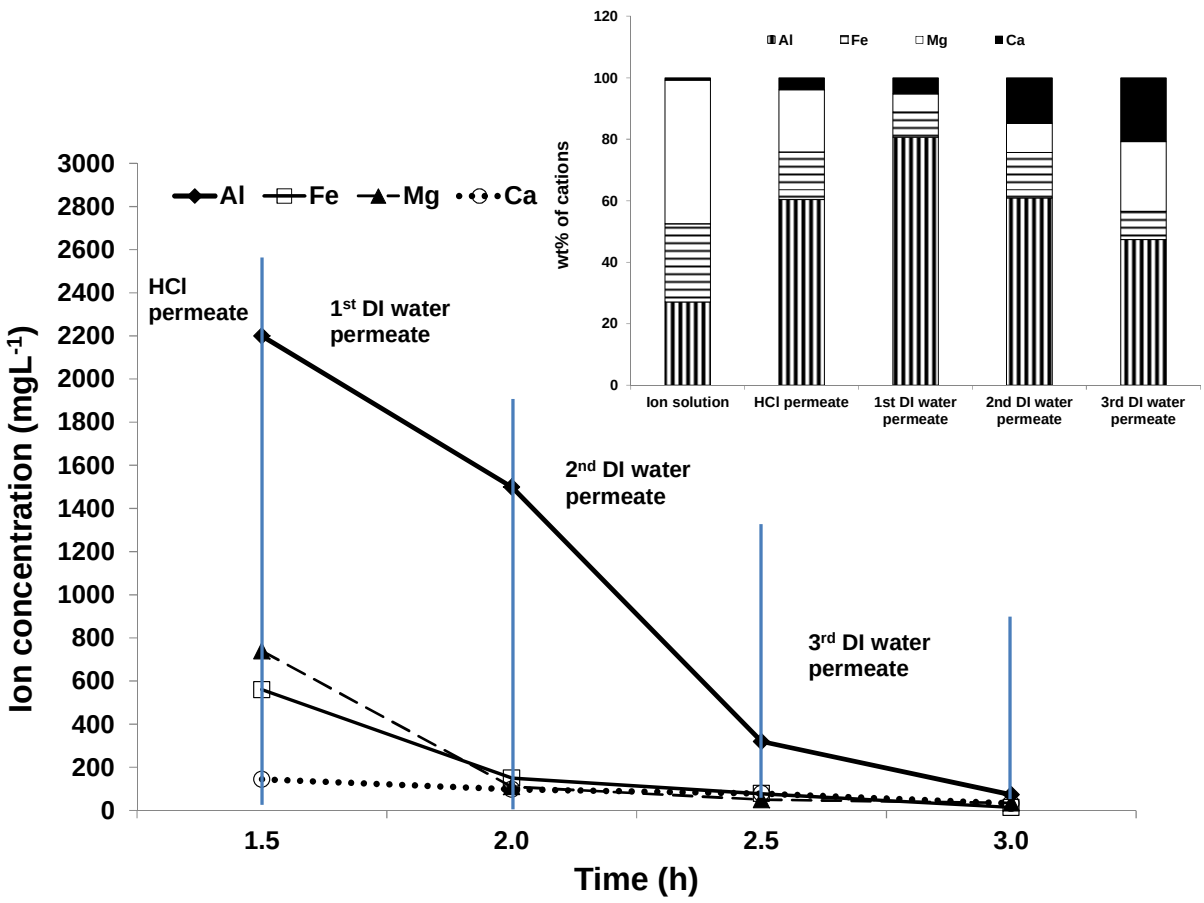

Fig. 6 Concentrations of cations (Fe^{3+}, Al^{3+}, $Ca^{2+}$and Mg^{2+}) measured for each permeate sample over time, and calculated proportions of the cations for the pre-filtered multivalent ion feed solution and the permeate samples (inset).

Table 6 Amount of the cations (Fe^{3+}, Al^{3+}, $Ca^{2+}$and Mg^{2+}) adsorbed by zeolite material in ion infiltration experiments, and removed from the multivalent ion solution tested membrane by 1 M HCl cleaning (HCl permeate) and DI water flushing (1^{st}, 2^{nd} and 3^{rd} DI water permeate).

Sample	Al^{3+} (mmol)	Fe^{3+} (mmol)	Mg^{2+} (mmol)	Ca^{2+} (mmol)
HCl permeate	0.0358	0.0044	0.0134	0.0016
1^{st} DI water permeate	0.0422	0.0021	0.0034	0.0019
2^{nd} DI water permeate	0.0116	0.0014	0.0020	0.0019
3^{rd} DI water permeate	0.0024	0.0002	0.0013	0.0007
Total removed from membrane	0.0921	0.0081	0.0201	0.0061
Adsorbed by zeolite powder	0.1852	0.1214	0.0001	0.0006

It appears that Al^{3+} and Ca^{2+} were released more in proportion from the zeolite compared to all other cations, even when cleaning with HCl that would remove more tightly bound ions (Fig. 6 inset). Ca^{2+} and Mg^{2+} can be regarded as not having a major role in the structure compared to the other ions, as only a very small amount was taken up by the zeolite according to powder infiltration study (Table 6). The interactions appear to be mostly controlled by Al^{3+} and Fe^{3+} as far greater quantities (Table 6) were taken up by the zeolite observed in the powder infiltration study. Fe^{3+} was proportionately lower in the permeates than Al^{3+} (Fig. 6 inset) and removed 10 time less from the membrane compared to Al^{3+} but showed the highest total amount (similar level to Al^{3+}) adsorbed in zeolite material in ion infiltration experiments (Table 6). Therefore, we conclude that Fe^{3+} has made the strongest association into the zeolite and cannot be removed readily either by DI water or HCl solution cleaning. Al^{3+} and Fe^{3+} being

multivalent and having higher charge density may bind more strongly into zeolite material initially, but interestingly only Fe^{3+} is not easily removed during HCl cleaning and DI water flushing, which implies it is the primary component responsible for rigid ion blocking of the membrane pores. It may be able to infiltrate and associate into more pores as it is smaller than Al^{3+} in hydrated form (Table 1). A trend of increasing proportion of Ca^{2+} present in the permeate samples (Fig. 6 inset) reveals another interesting finding, where although little Ca^{2+} was taken up into the zeolite (Table 6) its presence by proportion increases as the Al^{3+} is eventually washed out. Apart from the interactions between cations and zeolite material, SO_4^{2-} as the most dominant anion in our system might have also contributed the membrane pore blocking effect due to its significant size of 0.758 nm (Table 1). It was measured in the permeate from the HCl cleaning at 6,600 mg L^{-1} and the 1st DI water flushing at 3,120 mg L^{-1}, logically being the counter ion for the cations released.

Elemental analysis (Table 7) was also conducted by EDS on the zeolite membrane surface before and after ion infiltration test. It should be noted that the membrane being analysed by EDS was subjected to HCl solution and DI water permeation after the ion infiltration test. Therefore, the detection of ions after the ion infiltration test and acid and DI water cleaning indicates that the loosely bound ions were rinsed away, leaving only ions that were tightly bound with the zeolite structure. As shown in Table 7, Fe, Al and S were present in higher concentrations at the membrane surface after exposure to the multivalent ion solution. This confirmed that zeolites strongly interacted with ions present in ion solution during ion infiltration and the ions have penetrated into the zeolite structure (larger microporous grain boundaries and mesopores). The EDS results

also showed an overall reduction in Si proportion, indicating that the major ions from the ion solution were making up a larger proportion of the material. The other major ions (Mg^{2+} and Ca^{2+}) present in the ion solution were not detected within the exposed zeolite membrane. These results support the conclusions of the ion infiltration/acid solution and water leaching study, where Fe^{3+} was the most strongly incorporated and responsible for the pore blocking, while Ca^{2+} and Mg^{2+} did not have a major role in the zeolite structure. However, reasonably high amount of Al^{3+} was still present suggesting it has not been completely removed by acid cleaning and DI water flushing.

Table 7 EDS measured element contents on the zeolite membrane surface before and after exposure to the multivalent ion solution.

Element	Weight percentage before exposure	Weight percentage after exposure
O	50.97	51.92
Si	47.08	9.39
Fe	-	13.33
Al	1.19	12.44
S	-	10.69
Na	0.76	1.61
Mg	-	-
Ca	-	-
Br	-	0.62
Total	100	100

3.3 Evaluation of defect repair on zeolite membranes applied for desalination

To confirm the practical effect of the ion blocking treatment, improvement to desalination performance by the novel infiltration method applied to four randomly selected membranes produced in our labs was trialled. These membranes were taken from a set that showed at least a two orders of magnitude gas permeation ensuring that a zeolite layer had been formed and thus would be performance limited by defects within the zeolite film. The results are shown in Table 8. Various sizes of substrates were included in the trial, all coated with zeolite prepared by the same technique of seed rubbing and secondary growth. Here we can see that the infiltration made substantial improvements to the ability of the membrane to resist diffusion of salt in comparison to water (EC rejection rise). This was particularly important for the longer membranes of 300 mm length which are more prone to defect formation over the longer substrate length. In both of these cases, infiltration yielded a membrane with much higher EC rejection (up to 49%) from a membrane which exhibited little or no EC rejection initially. In all cases, however, a substantial loss in flux was observed which would be expected if the defect flow was inhibited by the blocking ions. Regardless, it appears that infiltration of the ion solution into the zeolite membrane using a setup that is essentially identical to simple reverse osmosis (pressurised flow) has consistently achieved improvement to the desalination performance compare to the as synthesised membrane. Blocking of gases was also observed (Table 5) but benefits to the more common application of zeolite membranes to gas separation (including organic molecules) and pervaporation (e.g. alcohol/water pervaporation) should be explored in

further work to fully validate this proposed infiltration technique more widely for zeolite membrane application.

Table 8 Comparison of desalination performance for MFI-type zeolite membranes before and after ion infiltration method

Membrane size ID×OD×length (mm)	Feed solution and total dissolved solids (mg L^{-1})	Test conditions	EC rejection (%)		Flux ($L\ m^{-2}\ h^{-1}$)	
			Before repair	After repair	Before repair	After repair
10×15×25	NaCl solution, 3,000	7 MPa 21 °C	17	70	2.8	0.3
10×15×300	Seawater, 35,000	7 MPa 21 °C	0	49	21	1.9
10×15×300	Seawater, 35,000	5 MPa 21 °C	3	25	6.0	1.4
25×30×158	NaCl solution, 3,000	0.5 MPa 21 °C	24	84	0.05	0.03

3.4 Mechanism of defect repair

Figure 7 shows a concept schematic of MFI-type zeolite membrane defect repair mechanism based on the findings from this investigation. The prepared zeolite membrane shows a low ion rejection and a high flux due to the existence of defect pores. When zeolite material is exposed to ion solution containing cations Al^{3+}, Fe^{3+}, Ca^{2+} and Mg^{2+}, it shows dynamic ion infiltration behaviour when interacting with the ions. The strong release of monovalent ions (e.g. K^{+}, Na^{+}) from zeolite material to accommodate multivalent ions (e.g. Fe^{3+}, Al^{3+}) from the ion solution yielded more open intrinsic pores and blockage of defect pores. The blocking of zeolite membrane defect pores by multivalent ions (Fe^{3+}, Al^{3+}) results in a high ion rejection but a reduced flux. This effect is of great use more widely in efforts to develop zeolite membranes where

transport through the zeolite cage governs separation, and zeolite pores are opened while grain boundaries are sealed. The strength of binding of Fe^{3+} into these grain boundaries appears to resist repetitive cleaning by acid and DI water suggesting a method for robust defect repair.

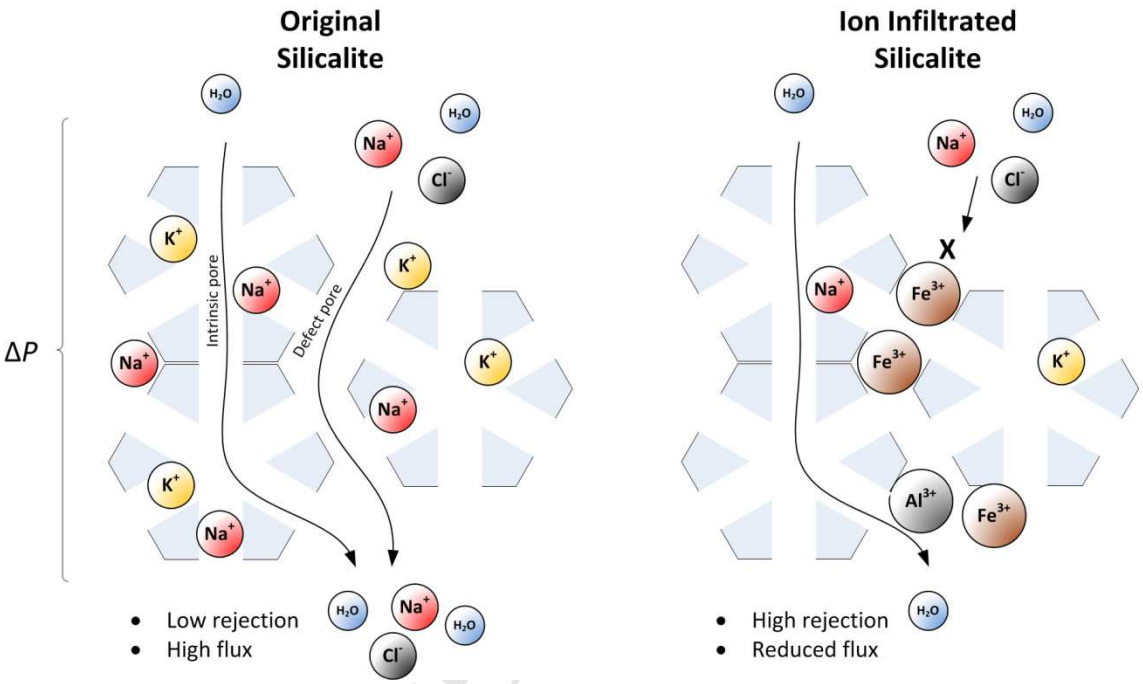

Fig. 7 Schematic illustration of ion interactions during zeolite exposure to ion solution containing cations Al^{3+}, Fe^{3+}, Ca^{2+} and Mg^{2+}.

The means by which the ions firmly anchor within the structure relates to the association of the ions with the zeolite surface. The ideal silicalite used in this work is not regarded as having sites for ion exchange due to the absence of alumina [29, 57], so ion co-ordination to the surface must be due to the silica surface physical and chemical properties. It is known that silanol groups (geminal, vicinal and isolated silanols) can form not only on the surface but also within the structure of silica, and the hydroxyl

(OH) groups are the main adsorption centres when interacting with the adsorbates [58, 59]. Similar to silica, Si–OH groups can also form either on the external surface of silicalite or within the zeolite lattice by adsorption of water molecules [60]. Ion adsorption can modify the surface, and the competition for adsorption sites by hydrated ion is governed by the relative degree of hydration, the size of the ion, the ion's valency and indeed the surface sites of attraction on the zeolite including the various arrangements of silanol groups [59]. The mechanism of ion association with the silica surface has been proposed according to [61]:

$$\text{Si-OH} + (H_2O)_xM^{y+} \rightarrow \text{Si-OM}^{(y-1)}+(H_2O)^{x-1} + H_2O + H^+ \quad (4)$$

where x is the number of water molecules associated with the metal ion, M, and y is the ion valency. This may be considered as the key association mechanism where no organic molecules are present. Ions with higher valency can associate with more sites enabling strong complexes to be formed, where adsorption of specific ions is dependent on the geometry of the co-ordination bonds that can be formed. It was also pointed out that adsorption of polybasic ions is essentially irreversible [61, 62], and chelation could involve surface silanol groups replacing water molecules from the metal ion as follows:

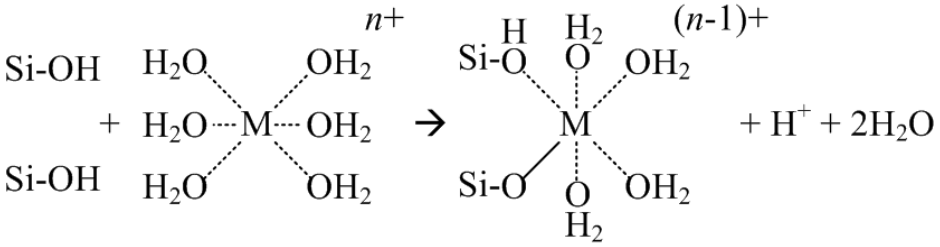

(5)

At pH of 2 and lower, certain polyvalent cations are strongly adsorbed on the silica surface, including Al^{3+} and Fe^{3+}. Further, it has been identified that these ions have a greater tendency to form covalent bonds compared to the other ions in the solution Ca^{2+}, Mg^{2+}, K^{+} and Na^{+} [63]. Therefore according to the research on ion interactions with silica surfaces, the procedure adopted to infiltrate the ions at pH 2 appears to have been a key part in favouring strong chelating behaviour of Al^{3+} and Fe^{3+} to the silicalite surface [61, 64]. Impurities need also to be considered, where it is known that Na and K impurities coming from zeolite synthesis (alkaline medium and template), or Al coming from the zeolite growth on the membrane (from Al_2O_3 support) [18, 36, 37]. These can be present also within the final zeolite. Na or K can take place of the silanol protons according to Equation 4, but when zeolite material is exposed to ion solution containing multivalent cations Al^{3+}, Fe^{3+}, Ca^{2+} and Mg^{2+}, the K^{+} and Na^{+} impurities inside the zeolite material were replaced by the multivalent ions (e.g. Fe^{3+}, Al^{3+}) due to their strong chelating capacity. The contamination from Al in the substrate of membranes can form isomorphic tetrahedral with an extra negative valence yielding a much stronger cation exchange capacity for the zeolite [58] which is well known for aluminosilicate zeolites including ZSM-5 [29, 65]. However this behaviour is not considered significant as the presence of Al in the original zeolite membrane was minor in comparison to Si according to EDS results (Table 7), and therefore the strong chelating effect of Fe^{3+} and Al^{3+} at low pH is more likely following the reported behaviours on pure silica.

4. Conclusion

This work investigated the role of multivalent ions for repairing defects in zeolite membrane films by first exploring the uptake of multivalent ions Fe^{3+}, Al^{3+}, Ca^{2+} and Mg^{2+} into MFI-type zeolite powders, followed by infiltrating the ions into a MFI-type zeolite membrane fabricated by the seeded secondary growth method. The change to crystal structure (shrinkage in the lattice) and the porous property (increase in proportion of micropores) as a result of the strong ion uptake was observed by XRD and N_2 porosimetry. This confirmed that the adsorbed trivalent ions exclusively occupied the larger microporous (grain boundaries) while the intrinsic pores of MFI-type zeolites become more open due to departed monovalent ions. The unique ion blocking effect, particularly for the irreversibly adsorbed Fe^{3+} as observed from acid and water leaching experiments, was verified on four membranes. These included scaled up membranes which would be more prone to defects due to their larger surface area. The technique could be utilised as a useful defect repair technique for zeolite membranes more widely.

Acknowledgment

This research was funded by the Australian Research Council through a Linkage Project (LP100200242), Chosun Refractories Co. Ltd. (Republic of Korea) and C.I. Ceramics (Aust.) Pty. Ltd. The authors would like to thank Dr Yong-Han Na (Chosun Refractories Co. Ltd.) and Mr Takanori Oishi (C.I. Ceramics (Aust.) Pty. Ltd.) for their ongoing support and willingness to discuss project related issues.

References:

[1] T. Humplik, J. Lee, S.C. O'Hern, B.A. Fellman, M.A. Baig, S.F. Hassan, M.A. Atieh, F. Rahman, T. Laoui, R. Karnik, E.N. Wang, Nanostructured materials for water desalination, Nanotechnology, 22 (2011) 292001.

[2] B. Zhu, D.T. Myat, J.-W. Shin, Y.-H. Na, I.-S. Moon, G. Connor, S. Maeda, G. Morris, S. Gray, M. Duke, Application of robust MFI-type zeolite membrane for desalination of saline wastewater, J. Membr. Sci., 475 (2015) 167-174.

[3] M. Duke, B. Zhu, C.M. Doherty, M. Hill, A.J. Hill, M.A. Carreon, Structural effects on SAPO-34 and ZIF-8 materials exposed to seawater solutions, and their potential as desalination membranes, Desalination, 377 (2016) 128–137.

[4] W.B. Samuel de Lint, T. Zivkovic, N.E. Benes, H.J.M. Bouwmeester, D.H.A. Blank, Electrolyte retention of supported bi-layered nanofiltration membranes, J. Membr. Sci., 277 (2006) 18-27.

[5] M.C. Duke, S. Mee, J.C. Diniz da Costa, Performance of porous inorganic membranes in non-osmotic desalination, Water Res., 41 (2007) 3998-4004.

[6] R. Xu, J. Wang, M. Kanezashi, T. Yoshioka, T. Tsuru, Development of robust organosilica membranes for reverse osmosis, Langmuir, 27 (2011) 13996-13999.

[7] A. Ikeda, E. Matsuyama, M. Komatsuzaki, M. Sasaki, M. Nomura, Development of inorganic silica reverse osmosis membranes by using a counter-diffusion chemical vapor deposition method, J. Chem. Eng. Jpn., 47 (2014) 574-578.

[8] M.C. Duke, J. O'Brien-Abraham, N. Milne, B. Zhu, J.Y.S. Lin, J.C. Diniz da Costa, Seawater desalination performance of MFI type membranes made by secondary growth, Sep. Purif. Technol., 68 (2009) 343-350.

[9] L. Li, J. Dong, T.M. Nenoff, R. Lee, Reverse osmosis of ionic aqueous solutions on aMFI zeolite membrane, Desalination, 170 (2004) 309-316.

[10] L. Li, J. Dong, T.M. Nenoff, R. Lee, Desalination by reverse osmosis using MFI zeolite membranes, J. Membr. Sci., 243 (2004) 401-404.

[11] L. Li, N. Liu, B. McPherson, R. Lee, Influence of counter ions on the reverse osmosis through MFI zeolite membranes: implications for produced water desalination, Desalination, 228 (2008) 217-225.

[12] N. Liu, L. Li, B. McPherson, R. Lee, Removal of organics from produced water by reverse osmosis using MFI-type zeolite membranes, J. Membr. Sci., 325 (2008) 357-361.

[13] L. Li, J. Dong, T.M. Nenoff, Transport of water and alkali metal ions through MFI zeolite membranes during reverse osmosis, Sep. Purif. Technol., 53 (2007) 42-48.

[14] Y. Deng, C. Deng, D. Qi, C. Liu, J. Liu, X. Zhang, D. Zhao, Synthesis of Core/Shell Colloidal Magnetic Zeolite Microspheres for the Immobilization of Trypsin, Adv. Mater., 21 (2009) 1377-1382.

[15] D.J. Doocey, P.N. Sharratt, C.S. Cundy, R.J. Plaisted, Zeolite-Mediated Advanced Oxidation of Model Chlorinated Phenolic Aqueous Waste: Part 2: Solid Phase Catalysis, Process Saf. Environ. Prot., 82 (2004) 359-364.

[16] W. Wang, M. Zhou, Q. Mao, J. Yue, X. Wang, Novel NaY zeolite-supported nanoscale zero-valent iron as an efficient heterogeneous Fenton catalyst, Catal. Commun., 11 (2010) 937-941.

[17] L.X. Li, J.H. Dong, T.M. Nenoff, R. Lee, Desalination by reverse osmosis using MFI zeolite membranes, J. Membr. Sci., 243 (2004) 401-404.

[18] L.X. Li, J.H. Dong, T.M. Nenoff, R. Lee, Reverse osmosis of ionic aqueous solutions on a MFI zeolite membrane, Desalination, 170 (2004) 309-316.

[19] L.X. Li, J.H. Dong, T.M. Nenoff, Transport of water and alkali metal ions through MFI zeolite membranes during reverse osmosis, Sep. Purif. Technol., 53 (2007) 42-48.

[20] M. Duke, J. O'Brien-Abraham, N. Milne, B. Zhu, Y.S. Lin, J.C. Diniz da Costa, Seawater desalination performance of MFI type membranes made by secondary growth, Sep. Purif. Technol., 68 (2009) 343-350.

[21] M. Kazemimoghadam, T. Mohammadi, Synthesis of MFI zeolite membranes for water desalination, Desalination, 206 (2007) 547-553.

[22] J. Lin, S. Murad, A computer simulation study of the separation of aqueous solutions using thin zeolite membranes, Mol. Phys., 99 (2001) 1175-1181.

[23] C.H. Cho, K.Y. Oh, S.K. Kim, J.G. Yeo, P. Sharma, Pervaporative seawater desalination using NaA zeolite membrane: Mechanisms of high water flux and high salt rejection, J. Membr. Sci., 371 (2011) 226-238.

[24] B. Zhu, J.H. Kim, Y.-h. Na, I.-S. Moon, G. Connor, S. Maeda, G. Morris, S. Gray, M. Duke, Temperature and pressure effects of desalination using a MFI-type zeolite membrane, Membranes, 3 (2013) 155-168.

[25] B. Zhu, Z. Hong, N. Milne, C.M. Doherty, L. Zou, Y.S. Lin, A.J. Hill, X. Gu, M. Duke, Desalination of seawater ion complexes by MFI-type zeolite membranes: temperature and long term stability, J. Membr. Sci., 453 (2014) 126–135.

[26] M. Drobek, C. Yacou, J. Motuzas, A. Julbe, L. Ding, J.C. Diniz da Costa, Long term pervaporation desalination of tubular MFI zeolite membranes, J. Membr. Sci., 415–416 (2012) 816-823.

[27] E.R. Nightingale Jr., Phenomenological theory of ion solvation. Effective radii of hydrated ions, J. Phys. Chem., 63 (1959) 1381-1387.

[28] B. Zhu, L. Zou, C.M. Doherty, A.J. Hill, Y.S. Lin, X.R. Hu, H.T. Wang, M. Duke, Investigation of the effects of ion and water interaction on structure and chemistry of silicalite MFI type zeolite for its potential use as a seawater desalination membrane, J. Mater. Chem., 20 (2010) 4675 - 4683.

[29] B. Zhu, C.M. Doherty, X. Hu, A.J. Hill, L. Zou, Y.S. Lin, M. Duke, Designing hierarchical porous features of ZSM-5 zeolites via Si/Al ratio and their dynamic behavior in seawater ion complexes, Microporous Mesoporous Mater., 173 (2013) 78-85.

[30] L. Li, N. Liu, B. McPherson, R. Lee, Enhanced Water Permeation of Reverse Osmosis through MFI-Type Zeolite Membranes with High Aluminum Contents, Ind. Eng. Chem. Res., 46 (2007) 1584-1589.

[31] Introduction to Reverse Osmosis Membrane, Available from: http://www.csmfilter.com/csm/upload/TechManual/Types.pdf (accessed August, 2016).

[32] FILMTEC™ Reverse Osmosis Membranes Technical Manual, The Dow Chemical Company ("Dow"), Form No. 609-00071-1009.

[33] Y. Liu, X. Chen, High permeability and salt rejection reverse osmosis by a zeolite nano-membrane, Phys. Chem. Chem. Phys., 15 (2013) 6817-6824.

[34] Z.E. Hughes, L.A. Carrington, P. Raiteri, J.D. Gale, A Computational Investigation into the Suitability of Purely Siliceous Zeolites as Reverse Osmosis Membranes, J. Phys. Chem. C, 115 (2011) 4063-4075.

[35] M. Noack, P. Kölsch, A. Dittmar, M. Stöhr, G. Georgi, R. Eckelt, J. Caro, Effect of crystal intergrowth supporting substances (ISS) on the permeation properties of MFI

membranes with enhanced Al-content, Microporous Mesoporous Mater., 97 (2006) 88-96.

[36] E.R. Geus, M.J. Den Exter, H. Van Bekkum, Synthesis and characterization of zeolite (MFI) membranes on porous ceramic supports, J. Chem. Soc., Faraday Trans., 88 (1992) 3101-3109.

[37] J. Dong, K. Wegner, Y.S. Lin, Synthesis of submicron polycrystalline MFI zeolite films on porous ceramic supports, J. Membr. Sci., 148 (1998) 233-241.

[38] J.S. Lee, J.H. Kim, Y.J. Lee, N.C. Jeong, K.B. Yoon, Manual Assembly of Microcrystal Monolayers on Substrates, Angew. Chem. Int. Ed., 46 (2007) 3087-3090.

[39] W.C. Yoo, J.A. Stoeger, P.-S. Lee, M. Tsapatsis, A. Stein, High-Performance Randomly Oriented Zeolite Membranes Using Brittle Seeds and Rapid Thermal Processing, Angew. Chem. Int. Ed., 49 (2010) 8699-8703.

[40] H. Rietveld, A profile refinement method for nuclear and magnetic structures, J. Appl. Crystallogr., 2 (1969) 65-71.

[41] C.A. Cooper, Y.S. Lin, Synthesis and characterization of silicalite powders and membranes with micro-meso bimodal pores, J. Mater. Sci., 42 (2007) 320-327.

[42] J. Li, J. Sun, Z. Li, H. Peng, D. Gidley, R. Todd, E., Y. Yan, Evaluation of pore structure in pure silica zeolite MFI low-k thin films using positronium annihilation lifetime spectroscopy, J. Phys. Chem. B, 108 (2004) 11689-11692.

[43] C. Baerlocher, L.B. McCusker, Database of zeolite structures: http://www.iza-structure.org/databases/ (accessed October, 2015).

[44] C. Andersson, J. Hedlund, Effects of exposure to water and ethanol on silicalite-1 membranes, J. Membr. Sci., 313 (2008) 120-126.

[45] H. Van Koningsveld, H. Van Bekkum, J.C. Jansen, On the location and disorder of the tetrapropylammonium (TPA) ion in zeolite ZSM-5 with improved framework accuracy, Acta Crystallogr., 43 (1987) 127-132.

[46] D.H. Olson, G.T. Kokotailo, S.L. Lawton, W.M. Meier, Crystal structure and structure-related properties of ZSM-5, J. Phys. Chem., 85 (1981) 2238-2243.

[47] F. Cailliez, N. Desbiens, A. Boutin, I. Demachy, M. Trzpit, M. Soulard, J. Patarin, A.H. Fuchs, Thermodynamic study of water intrusion in hydrophobic zeolites by Monte Carlo simulations, in: A. Gédéon, P. Massiani, F. Babonneau (Eds.) Studies in Surface Science and Catalysis, Volume 174, Part A, Elsevier, 2008, pp. 683-688.

[48] M. Noack, M. Schneider, A. Dittmar, G. Georgi, J. Caro, The change of the unit cell dimension of different zeolite types by heating and its influence on supported membrane layers, Microporous Mesoporous Mater., 117 (2009) 10-21.

[49] M. Kuronen, M. Weller, R. Townsend, R. Harjula, Ion exchange selectivity and structural changes in highly aluminous zeolites, React. Funct. Polym., 66 (2006) 1350-1361.

[50] G. Vezzalini, A. Alberti, A. Sani, M. Triscari, The dehydration process in amicite, Microporous Mesoporous Mater., 31 (1999) 253-262.

[51] K.S.W. Sing, D.H. Everett, R.A.W. Haul, L. Moscou, R.A. Pierotti, J. Rouquerol, T. Siemieniewska, Reporting physisorption data for gas/solid systems, Pure Appl. Chem., 57 (1985) 603—619.

[52] H. Li, Y. Sakamoto, Z. Liu, T. Ohsuna, O. Terasaki, M. Thommes, S. Che, Mesoporous silicalite-1 zeolite crystals with unique pore shapes analogous to the morphology, Microporous Mesoporous Mater., 106 (2007) 174-179.

[53] H. Wang, Z. Wang, L. Huang, A. Mitra, B. Holmberg, Y. Yan, High-surface-area zeolitic silica with mesoporosity J. Mater. Chem., 11 (2001) 2307-2310.

[54] S.J. Jung, M.H. Kim, H.D. Kim, Y.H. Kim, S.R. Kim, Synergy between microwave irradiation and promoter addition about synthesis of nanosized TPA-silicalite-1, in: E. van Steen, I.M. Claeys, L.H. Callanan (Eds.) Studies in Surface Science and Catalysis, Elsevier, 2004, pp. 180-183.

[55] H. Ajot, C. Russmann, J.F. Joly, H. Kessler, Revealing Zeolite Microporosity During Organic Template Removal, in: F. Rodríguez-Reinoso, J. Rouquerol, K. Unger, K.S.W. Sing (Eds.) Studies in Surface Science and Catalysis, Elsevier, 1994, pp. 477-485.

[56] J. O'Brien-Abraham, M. Kanezashi, Y.S. Lin, A comparative study on permeation and mechanical properties of random and oriented MFI-type zeolite membranes, Microporous Mesoporous Mater., 105 (2007) 140-148.

[57] S. Sircar, A.L. Myers, Gas Separation by Zeolites, in: S.M. Auerbach, K.A. Carrado, P.K. Dutta (Eds.) Handbook of Zeolite Science and Technology, CRC Press, New York, 2003, pp. 1354-1406.

[58] H.E. Bergna, Colloid Chemistry of Silica, The Colloid Chemistry of Silica, American Chemical Society, 1994, pp. 1-47.

[59] L.T. Zhuravlev, The surface chemistry of amorphous silica. Zhuravlev model, Colloids Surf., A: Physicochemical and Engineering Aspects, 173 (2000) 1-38.

[60] A. Özgür Yazaydın, R.W. Thompson, Molecular simulation of water adsorption in silicalite: Effect of silanol groups and different cations, Microporous Mesoporous Mater., 123 (2009) 169-176.

[61] R.K. Iler, The Chemistry of Silica: Solubility, Polymerization, Colloid and Surface Properties and Biochemistry of Silica, John Wiley and Sons., New York, 1979.

[62] H.P. Boehm, Chemical Identification of Surface Groups, in: H.P. D.D. Eley, B.W. Paul (Eds.) Advances in Catalysis, Academic Press, 1966, pp. 179-274.

[63] T. Wakatsuki, H. Furukawa, K. Kawaguchi, Specific and non-specific adsorption of inorganic ions I. Evaluation of specific adsorbability by means of minimum concentration for specific adsorption, J. Soil Sci. Plant Nutr., 20 (1974) 353-362.

[64] P.W. Schindler, B. Fürst, R. Dick, P.U. Wolf, Ligand properties of surface silanol groups. I. surface complex formation with Fe^{3+}, Cu^{2+}, Cd^{2+}, and Pb^{2+}, J. Colloid Interface Sci., 55 (1976) 469-475.

[65] P. Chu, F.G. Dwyer, Inorganic Cation Exchange Properties of Zeolite ZSM-5, in: G.D. Stucky, F.G. Dwyer (Eds.) Intrazeolite Chemistry, American Chemical Society, 1983, pp. 59-78.

Supplemental material

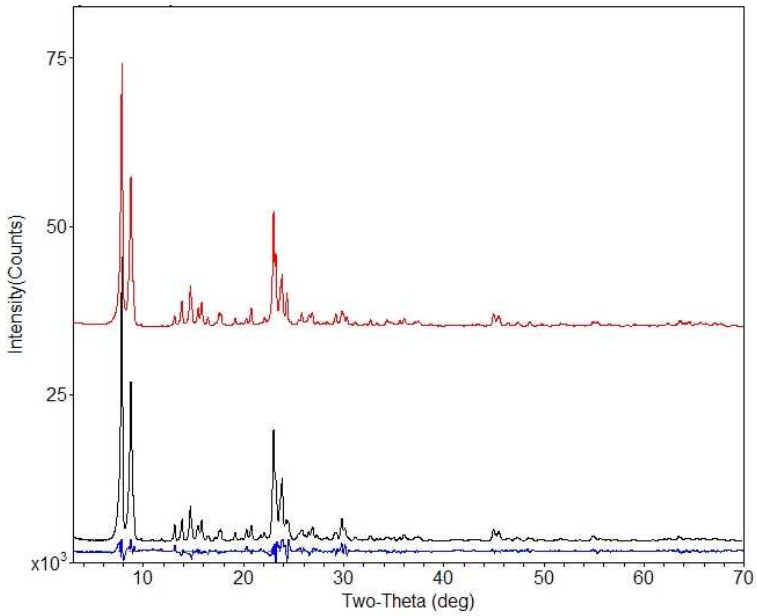

Fig. S1 Rietveld plots for the original MFI-type zeolite powder samples. Upper trace: calculated, middle trace: observed and lower trace: difference between the calculated and observed profiles.

Highlights:

- A unique ion blocking for defect repair of MFI-type zeolite membranes was revealed.
- Improvement to desalination performance was verified on defect repaired membranes.
- The technique could be utilised for defect repair of zeolite membranes more widely.